A CLOSE-UP LOOK AT IO FROM GALILEO'S NEAR-INFRARED MAPPING SPECTROMETER

Rosaly Lopes-Gautier*, S. Douté, W.D. Smythe, L.W. Kamp, R.W. Carlson, A.G. Davies, F.E. Leader, A.S. McEwen, P.E. Geissler, S.W. Kieffer, L. Keszthelyi, E. Barbinis, R. Mehlman, M. Segura, J. Shirley, L.A. Soderblom

Rosaly Lopes-Gautier, E. Barbinis, R.W. Carlson, A.G. Davies, L.W. Kamp, M. Segura, J. Shirley, W.D. Smythe, Jet Propulsion Laboratory, California Institute of Technology, Pasadena, CA 91109.
S. Douté, F. Leader, R. Mehlman, IGPP, University of California, Los Angeles, CA 90095.
S. W. Kieffer, Kieffer & Woo, Inc., PO Box 130, Palgrave, Canada LON 1PO.
P. E. Geissler, A.S. McEwen, L. Keszthelyi, Lunar and Planetary Laboratory, University of Arizona, Tucson, AZ 85721.
L. Soderblom, U.S.Geological Survey, Flagstaff, Arizona 8600.

* To whom correspondence should be addressed. Email: rlopes@lively.jpl.nasa.gov

Infrared spectral images of Jupiter's volcanic moon Io, acquired during October and November 1999 flybys of the Galileo spacecraft, were used to study the thermal structure and sulfur dioxide distribution of active volcanoes. Loki Patera, the solar system's most powerful known volcano, exhibits large expanses of dark, cooling lava on its caldera floor. Prometheus, the site of long-lived plume activity, has two major areas of thermal emission, which support ideas of plume migration. Sulfur dioxide deposits were mapped at local scales and show a more complex relationship to surface colors than previously thought, indicating the presence of other sulfur compounds.

A major objective of the Galileo mission was to investigate Io's volcanoes and their surface modification processes using high spatial resolution spectral images. Observations were obtained during two flybys of Io in October 1999 (orbit I24) and November 1999 (orbit I25) using the near-infrared mapping spectrometer (NIMS). It was known previously that Io's surface is dotted with active volcanoes (hot spots) (1), and covered by SO_2 frost and other compounds (2,3,4). Some hot spots exhibit plumes that may inject gaseous SO_2 into the atmosphere (5), subsequently condensing as frost on the surface.

NIMS obtained 17 observations during I24 and 4 observations during I25, most with spatial resolutions from 0.5 to 25 km/NIMS pixel. These were obtained at 14 fixed infrared (IR) wavelengths (in the range from 1.0 to 4.7 μm) instead of the planned 360, because the instrument's spectral scanning capability malfunctioned. This anomalous

operation provided greater sampling density (24 samples instead of 1) at each wavelength, increasing the signal/noise ratio. The reduced number of wavelengths is suitable for temperature determination and SO_2 mapping, but our search for yet unknown surface compounds was compromised.

The NIMS spectral range includes reflected sunlight and thermal emission components (Supplementary Figure 1). A pixel showing volcanic activity may contain lavas at different temperatures (6), but here we use a single-temperature Planck function to estimate the brightness temperature T_B and the color temperature T_C, with a correction for reflected sunlight in daytime observations (7). T_B is a measure of the average emitted thermal energy within a given wavelength interval and pixel area. T_C uses the shape and amplitude of the Planck function to determine a temperature and its corresponding emitting area within the pixel. T_C estimates tend to be dominated by cooler materials that typically cover larger areas and thus emit greater power (in the wavelength range used) than the hotter materials having much smaller areas.

For SO_2 mapping, the reduced number of wavelengths precluded the full-spectrum modeling used previously (3). We used the 4.1-μm spectral channel, which lies within the strong SO_2 $\nu_1 + \nu_3$ absorption band (Supplementary Figure 1), as a qualitative SO_2 indicator. Specifically we form the relative band depth from the absorption depth at 4.1 μm relative to measurements at a non-absorbing wavelength (3.0 μm) (8). The relative band depth depends on the SO_2 abundance, the mean grain size, and the presence of other materials and their mixing mode (spatially segregated or intimately mixed at the scale of photon path lengths). Here we assume spatially segregated mixing. SO_2 absorbs strongly at 4.1 μm (absorption coefficient ~ 11 cm^{-1}, Ref. 9) so non-zero reflectance at that wavelength indicates the presence of other, non-absorbing material. The assumption of spatially segregated mixing (10) with spectrally neutral material gives upper bounds to the SO_2 abundance. The depth of sampling at 4.1 μm-wavelength is limited to about 1mm, so we cannot distinguish between thick frost deposits and thin layers (that can be transparent in the visible and at non-absorbing IR wavelengths).

Loki Patera: NIMS imaged Loki Patera on Io's nightside, targeting a light-colored, island-like feature in the caldera (Fig. 1). This feature has not changed significantly in appearance (at scales of several kilometers) since 1979. It is cut by a dark-colored, linear feature about 3.5 km wide that may be a crack exposing dark lava, or a valley flooded by lava. Additional NIMS data on and beyond the caldera floor, having lower spatial sampling density, were obtained as the spacecraft's scan platform moved to the next target. Temperature maps (Fig. 1) show that the island and the light terrain outside the caldera exhibit low thermal emission (no T_C fits to these data were attempted), while the dark floor of the caldera and the crack have higher thermal output. The dark caldera floor is quite uniform in brightness temperature (273±6K), with 70% of the pixels having median T_B's of 273±2 K. Median T_B's for the crack material are lower (215±10K). However, median T_C's for the material in the crack are higher (350±55K) than those for floor (305±44K). This indicates that the area of the hot crack is smaller than the size of the NIMS pixel with most of the contribution for the T_B map arising from the cooler material. The areas corresponding to T_C's can be obtained. For a pixel on the crack at the

median T_C, the area is 0.0065 km^2 (0.28% of the pixel area that could be represented as a linear feature 4.3 m wide by the length of the pixel, 1.5 km). For a pixel on the floor, the area is 0.655 km^2 (28.5 % of the pixel area).

The caldera floor's temperature distribution shows that it is uniform in terms of energy output (similar T_B's) but at a scale below the size of individual pixels (T_C's) the lavas show a more complex structure. This is consistent with a field of overlapping, cooling lava flows, or with the cooling, non-uniform surface of a lava lake. Observations by Galileo's photopolarimeter radiometer (11), taken at longer wavelengths, also show little variation in temperature on the eastern caldera floor, but show higher temperatures near the southwestern edge of the caldera and extending to the west of the island, regions not observed by NIMS. This is near the site of an eruption that begun in early September 1999 (11). The lavas observed by NIMS on the caldera floor were probably emplaced during an earlier eruption. If the lava were erupted at 1475 K (typical for basaltic lavas), and were at least 5 m thick, the time (under Io conditions) for the lava to cool down to the median T_C for the caldera floor (305 K) would be about 127 days (12). However, the lava would only need about 39 days to cool down to the median T_C for the crack (350 K), so it is possible that the lavas in the crack were emplaced during the earlier phase of the September 1999 eruption.

Tvashtar Catena: This chain of calderas were observed by NIMS and SSI in I25, and almost simultaneously from the ground. The ground-based (13) and SSI observations (14) were interpreted as images of a fire fountain erupting hot lavas. The observation by NIMS covers the eastern part of the active caldera and the pixels at most wavelengths are saturated. The hottest pixel for which a temperature could be derived (which is cooler than the hottest pixel observed) yielded T_C=1060±60 K (area=0.003 km^2). This estimate can mask small areas having high temperatures and is a lower limit that, although well within the range of basaltic lava temperatures, does not exclude ultramafic compositions such as those observed at Pillan Patera (15). Data just returned from the third Io flyby (I27) show that activity had fallen to a lower level by February 2000. NIMS pixels from the same locations as in I25 do not show saturation and yield temperatures between 500 and 600 K.

Prometheus: Prometheus is the site of a persistent plume discovered by Voyager in 1979 (5). Observations by SSI during Galileo's first orbit in 1996 showed that the Prometheus plume site had moved about 80 km west since 1979 (16), but the size and appearance of the displaced plume had not changed. Observations by SSI in I24 showed a caldera just to the north of the Voyager plume site (14), and a long lava flow between the Voyager and Galileo plume sites. The NIMS observation of the same region (Fig. 2) showed 2 main hot spots, though thermal emission can be detected along the flow. The eastern hot spot is near the location of the 1979 plume, while the western hot spot is at the location ~~of the~~ current plume. The eastern hot spot is ~~hotter but~~ smaller in area (T_C=840±??? K, area = 0.007 km^2) than the western hot spot (T_C=520±??? K, area = 0.08 km^2). Values obtained for a pixel between the two hot spots yielded T_C=420±??? K. This temperature distribution is consistent with that of a lava flow being erupted from the eastern hot spot, which cools and becomes crusted over as it moves away from the vent.

note : will be corrected

Hot lava can flow through tubes and break out at the distal edge of the flow, spreading out over the surface, with hot material spreading over a larger area than at the vent. The vent associated with the eastern hot spot did not move. Instead, the plume moved to the western hot spot, even though the eastern hot spot remained active. This could arise from an interaction between hot lava and the underlying SO_2 snowfield (17).

The deposition of material from the Prometheus plume was mapped from a NIMS observation at spatial resolution of 20-25 km/NIMS pixel (Fig. 3). Thermal emission and SO_2 absorption can be seen at 4.1 μm (Fig. 3B). The SO_2 relative depth map (Fig. 3C) has been translated into a SO_2 distribution map (Fig. 3D), using the linear correlation between the relative depth and the SO_2 frost coverage (16). A striking feature (Fig. 3D) is the SO_2 deposition ring that circles the vent. When compared with the low-phase visible image (Fig. 3A), the SO_2 deposition ring appears larger than its visible white counterpart. This suggests that Prometheus emits several different compounds (such as S_8) in the gas phase, that condense with a deposition distance from the vent inversely related to volatility. Before the flybys, it was thought that areas that were bright and white at low phase angles corresponded to regions rich in coarse-grained SO_2 (2,4). Our observation suggests that some other white material may be present.

Faint hot spots and vents: Several hot spots other than Prometheus are visible in this image (Fig. 3B). Camaxtli and Culann Patera had been detected before (1,16) but, at this higher spatial resolution, their complex structures are revealed. Culann Patera appears to have two separate hot spots within the same volcanic complex, while the Camaxtli Patera hot spot has two neighboring, small hot spots that may be independent volcanic centers. Six other relatively small and faint hot spots, which could not be seen in the global-scale observations, were detected (18). Brightness temperatures for the faint hot spots are ~220 K, and >270K for the brighter hot spots that had been detected at low spatial resolution. One of the faint, previously undetected hot spots coincides with the feature Chaac Patera, a distinct green region in visible images (4). This hot spot became active sometime between the two fly-bys. NIMS data from I24 showed no thermal emission from Chaac Patera, but an observation at comparable spatial resolution in I25 showed that it had become active and that a region to the northwest of this hot spot had become darker at the shorter NIMS wavelengths. Dark materials on Io correlate with volcanic activity, as noted in previous studies (19), including those from NIMS and SSI images at low spatial resolution (1,4). Comparison of Figures (3A) and (3B) illustrates this correlation well, as areas of low-albedo deposits in (3A) coincide with areas of enhanced thermal emission which appear bright in (3B).

Culann Patera and Tohil Patera: The hot spot Culann (Fig. 4) and the Tohil region (where no hot spot has so far been detected) show distinct red deposits. SO_2 relative depth maps superimposed on SSI images show locally enhanced concentrations of SO_2 that coincide with deposits having a pinkish-white to red appearance at visible wavelengths. Red deposits may be short-chain sulfur compounds (20) and are generally associated with hot spots (1,4). This intimate association of compounds having different volatility requires a particular emission or deposition mechanism that prevents their spatial segregation. A higher S_2/SO_2 ratio than that at Prometheus, for example, can lead

to a dense atmospheric population of radiatively cooled S_2 solid nuclei on which SO_2 condenses. Alternatively, boiling liquid SO_2 with short-chain sulfur or other coloring agents dissolved in it may reach the surface from below and freeze before complete sublimation. The diffuse appearance of the red deposits may arise from the entrainment of liquid droplets with escaping gases.

FIGURES:

FIGURE 1: NIMS observation over Loki Patera obtained during the I24 flyby, superimposed on a SSI image. Top: Brightness temperature map, showing that the temperatures for the lavas on the caldera floor are fairly uniform and hotter (red) than those for materials on the "island" and on the outside of the caldera. Bottom: Color temperature map, showing higher temperatures (reds and yellows) in the "crack" or valley that runs through the light-colored "island" in the center of the caldera. The small hot areas in the "crack" appear cool in brightness temperature because of their small size relative to the pixel. NIMS spatial resolution ranges from 1.3 to 2.1 km/pixel (21) and the SSI image is 162 km across.

FIGURE 2: Color temperature map (A) made from NIMS data obtained during the I24 flyby, at spatial resolution of 5.5 to 8.5 km/pixel (21). The SSI image (B), taken in July 1999, is 142 km across. Two major hot spots are seen in (A): the eastern hot spot, which has higher temperatures, is located near the site of the Voyager-era plume. The western hot spot coincides with the location of the currently active plume.

FIGURE 3: Prometheus region imaged by SSI in July 1999 (A) and by NIMS at 4.1 μm during the I24 flyby (B). The NIMS observation is at spatial resolution of 22 to 25 km/pixel (21). Hot spots appear red in (B), while SO_2 appears blue. Hot spots are labeled 1 (Prometheus), 5 (Camaxtli), 7 (Tupan) and 8 (Culann). Hot spots 2, 3, 4 and 6 were not previously known. The color-bar scale in (B) represents radiance in units of bidirectional

reflectance (solar irradiance/pi). The SO_2 deposition ring around Prometheus is clearly seen in the center of (B) and in (C), the relative band-depth map (8). A qualitative SO_2 distribution map is shown in (D). The color-bar scale gives the fractional area covered by SO_2 frost and varies from 0 (very dark blue) to 1 (yellow). The area shown in each panel is ~1300 km across.

FIGURE 4: NIMS obtained data over Culann Patera during the I25 flyby. An SO_2 relative band depth map (8) is shown over a SSI image acquired in July 1999. NIMS data shows enhanced concentrations of SO_2 coinciding with deposits that are pink to red in visible wavelengths. Spatial resolution is 11 km/pixel (21) and the SSI image is 340 km across. The color scale is the same as in Fig. 3C.

NOTES AND REFERENCES:

1. R. Lopes-Gautier et al., *Icarus*, **140**, 243 (1999).

2. R.W. Carlson et al.,*Geophys. Res. Lett.* **24**, 2479-82 (1997).

3. S. Douté et al., submitted to *Icarus* (1999).

4. P.E. Geissler et al., *Icarus* **140**, 265 (1999).

5. R.G. Strom and N.M. Schneider, in *Satellites of Jupiter*, D. Morrison, Ed. (University of Arizona Press, Tucson, AZ, 1982), pp. 598-633.

6. A.G. Davies et al. 1999, *Lunar Planet. Sci.* **XXX** (1999) [available on CD-ROM].

7. The brightness temperature, T_B, is defined as: $B(\lambda, T_B) = I(\lambda)$, where B is the Planck function, λ is the wavelength, and I is the corrected radiance.
The corrected radiance is defined as: $I(\lambda) = I_o(\lambda) - A * F(\lambda)$, where $I_o(\lambda)$ is the observed radiance, $F(\lambda)$ is incident solar flux at that wavelength and A is an albedo estimate derived from the 1 to 2 micron region. For nightside observations, $I=I_o$.
The color temperature, T_C, is defined as:
$B(\lambda_1, T_C) / B(\lambda_2, T_C) = I(\lambda_1)/I(\lambda_2)$
We used two pairs of (λ_1, λ_2): (4.1, 4.4 μm) and (4.4, 4.7 μm). The reported T_C is the average between the two values. In dayside observations, T_B and, in particular, T_C, are sensitive to the albedo used to correct the observed radiances, both in absolute value and its spectral slope (due to the SO_2 absorption at 4.1 μm). Therefore, calculations are made using a range of albedos, typically 60% to 80% of the value obtained at short wavelengths. The results are then averaged. Results displaying a high sensitivity to this variation (typically when $T_B < 200K$) are omitted, as are those in which the error between the two estimates of T_C exceeds 20% of the mean. T_C is only calculated for pixels in which T_B exceeds a threshold (usually 210 to 250 K, depending on the noise level), to avoid errors due to the SO_2 absorption, since this absorption disappears at hot spots.
Correct albedo values should yield $I(\lambda)=0$ for the cold areas of Io. Small residual uncertainties in the NIMS calibration can sometimes yield a spurious T_B ~180K for these areas, but pixels where $T_B<200K$ were not used in this analysis.

8. The relative band depth is defined as the ratio [A(3.0)/A(4.1)], where $A(\lambda)$ is the measured albedo (reflectance) at wavelength λ. This ratio was not obtained for pixels in which thermal emission could be detected.

9. B. Schmitt et. al., *Icarus 111*, 79 (1994), and B. Schmitt et al, in *Solar System Ices*, B. Schmitt, C. De Bergh, and M. Festou, Eds. (Kluwer Academic Publ., Dordrecht, 1998), pp. 199-240.

10. We have checked and quantitatively calibrated this simple approach (segregated mixing and linear combination of computed radiances) by comparing the relative band

depth map of a global observation taken in I24 with the SO_2 distribution maps of S. Doute' et al. (3), which modeled 408-wavelength NIMS spectra.

11. J. R. Spencer et al. (2000), this volume.

12. Times calculated using the model of A.G. Davies, **Icarus** *124*, 45 (1996). These temperatures and cooling rates assume that the surface heat loss is buffered by the release of latent heat from a still-molten flow interior.

13. R. Howell et al., *Lunar Planet. Sci.* **XXXI** (2000) [available on CD-ROM].

14. A.S. McEwen et al. (2000), this volume.

15. A.S. McEwen et al., *Science* **281**, 87 (1998).

16. A.S. McEwen et al., *Icarus* **135**, 181 (1998).

17. S.W. Kieffer et al., (2000), this volume.

18. Previously undetected hot spots detected by NIMS during I24 and I25 are located at: (+21, 146W, near Surya), (+14, 150 W), (+20, 149W), (+12, 158W, near Chaac), (-5, 132W, the dark feature Seth), and (+9, 133W)

19. J.C. Pearl and W.M. Sinton, in *Satellites of Jupiter*, D. Morrison, Ed. (University of Arizona Press, Tucson, AZ, 1982), pp. 724-755.

20. Spencer, J.R. et al. 1997, *Icarus* **127**, 221-37.

21. The pixel size in NIMS processed images is 0.5 x the instrument's spatial resolution.

22. Portions of this work were performed at the Jet Propulsion Laboratory, California Institute of Technology, under contract with the National Aeronautics and Space Administration.

Fig 1 (originally in color)

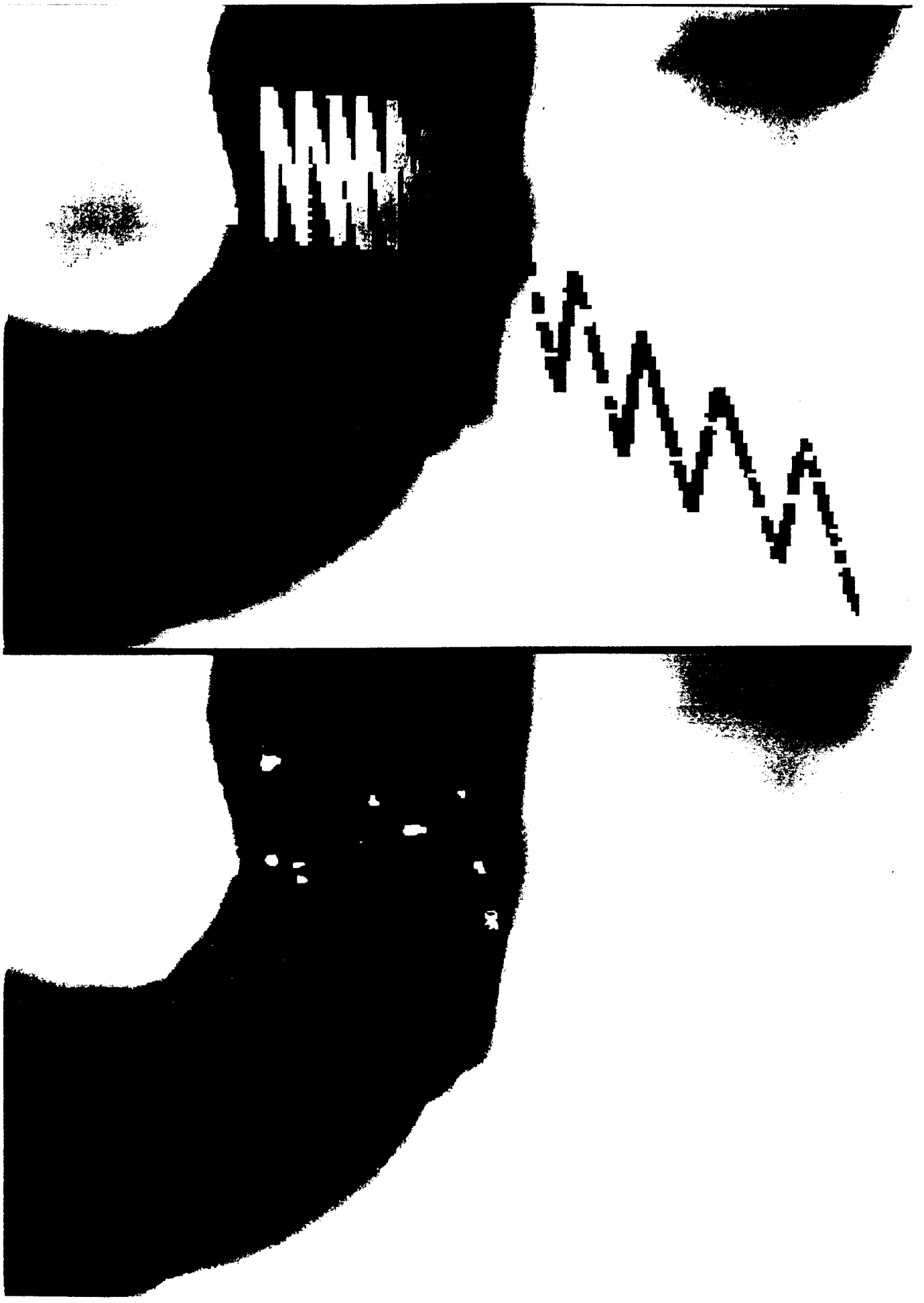

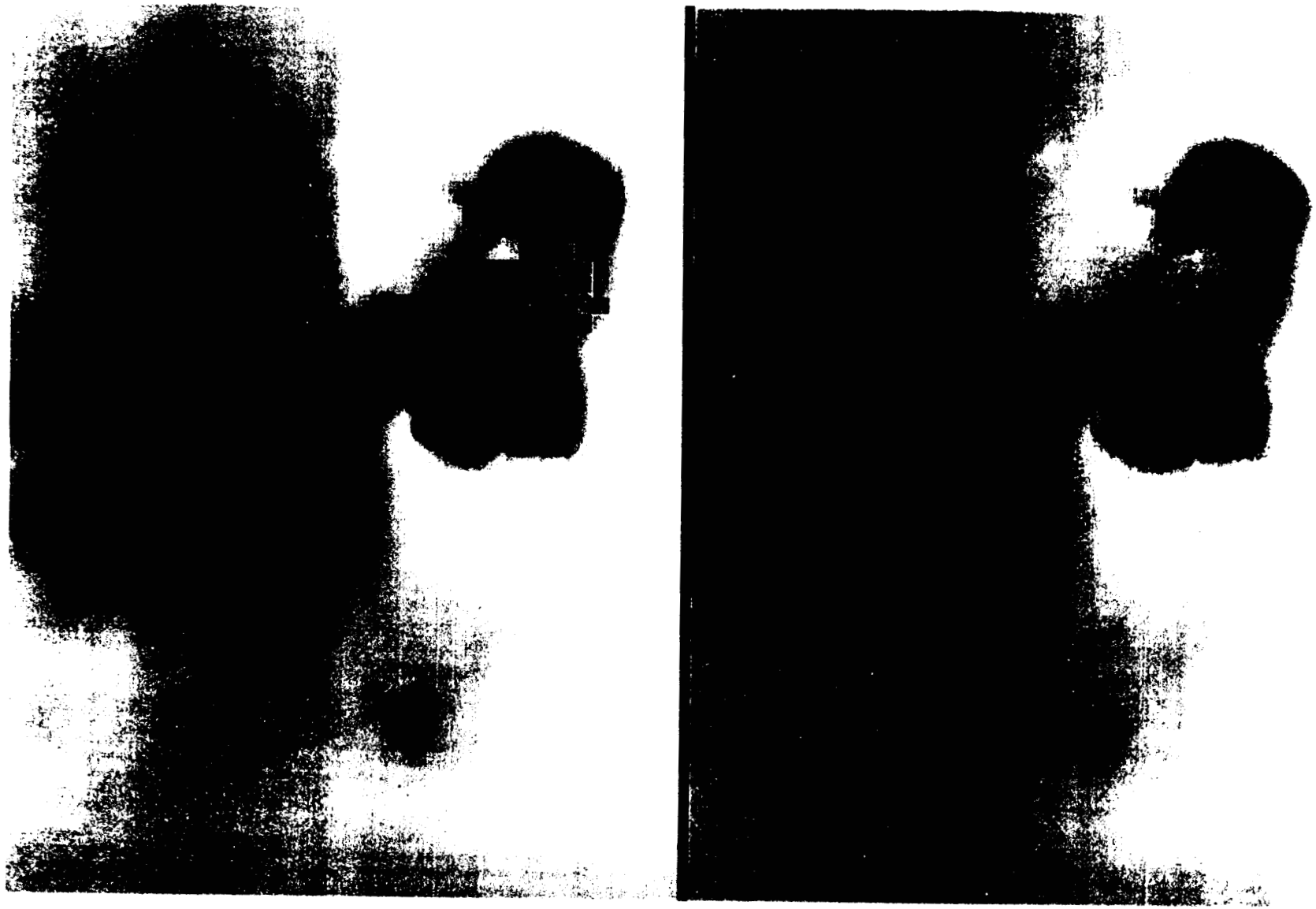

Fig 2 (original in color)

0.40
0.50
0.40
0.50
0.50
0.30
0.50

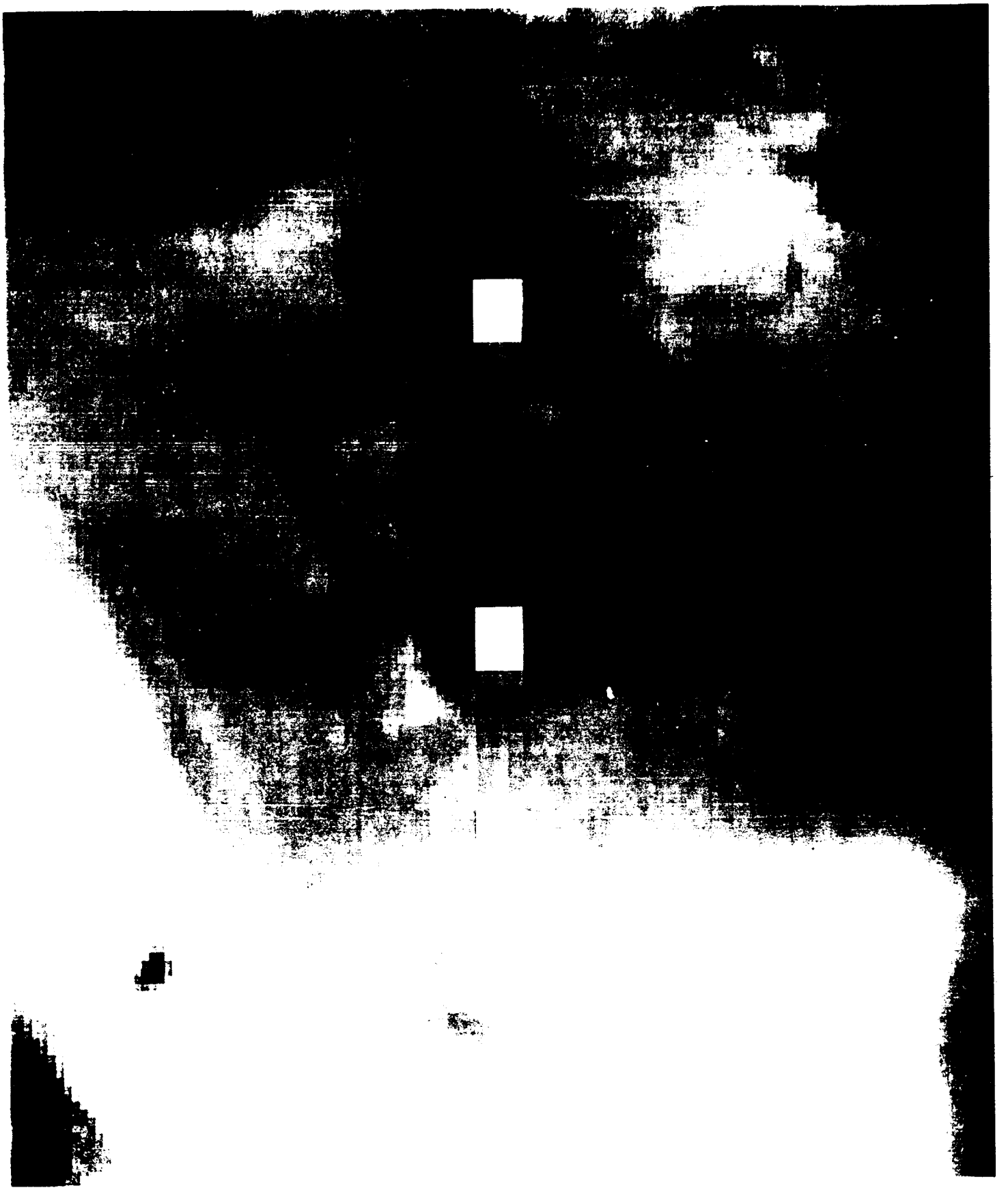

Supplementary Fig 1